Efficient Estimation of Electrical Machine Behavior by Model Order Reduction

Fabian Müller, Andreas Siokos, Johann Kolb, Martin Nell, and Kay Hameyer

Institute of Electrical Machines, RWTH Aachen University, 52062 Aachen, Germany

The proper orthogonal decomposition (POD) is an efficient model order reduction method, which is frequently coupled with the discrete empirical interpolation method (DEIM) to solve nonlinear electromagnetic problems. A drawback of this method is that instabilities can occur related to the reduction operator of the nonlinear part. In this contribution, different DEIMs and the Gappy POD are employed and analyzed. Consecutively, the methods are employed to efficiently estimate the behavior of a permanent magnet synchronous machine in terms of global quantities, such as torque and iron losses.

Index Terms— **Discrete empirical interpolation, finite element method, Gappy POD, iron losses, model order reduction, permanent magnet synchronous machine, proper orthogonal decomposition (POD).**

I. Introduction

THE simulation of electrical machines is a computationally demanding task due to solving large systems of equations arising from the electromagnetic field equations. Therefore, it is an ongoing aspiration to develop and employ mathematical models to reduce this effort. The proper orthogonal decomposition (POD) is a well-known reduction technique that can significantly reduce the degrees of freedom (DOFs) of linear and non-linear systems. However, in non-linear simulations, the computation saving is canceled by the necessity to evaluate the nonlinearity in the reference system. Employing the discrete empirical interpolation method (DEIM) copes with this additional burden but can introduce instabilities and inaccuracies in the system [2], [9], [10]. The Gappy POD was used to solve an eddy current problem in [10] and showed a more stable behavior. To reduce the instabilities, the truncated DEIM approach and the Gappy POD are compared. In addition, a localized DEIM (LDEIM) is employed, which uses different projections depending on the angular displacement of the rotor to further exploit any periodicity in local states of material saturation. Consecutively, the techniques are applied to a technical relevant example of a permanent magnet synchronous machine, and the accuracy and efficiency of the model order reduction methods are evaluated.

II. Magnetostatic Field Problems

Modeling of low-frequency electromagnetic fields, such as in electrical machines, is conducted by the finite element method. In an abstract context, the geometry can be considered as a bounded domain Ω, which is placed in $\mathbf{R}^2$. The domain may hold unary and binary boundaries and an interface to model the movement, which, in this case, is considered by a sliding interface [4]. The static version of Ampère's law is used to determine the magnetic vector potential A in electrical machines, where the eddy current effects are negligible

$$\nabla \times \nu(\nabla \times \boldsymbol{A}(\boldsymbol{x}, \theta)) = \boldsymbol{J}_{\text{Dens}}(\boldsymbol{x}, \theta) + \nabla \times \nu \boldsymbol{B}_{\text{PM}}(\boldsymbol{x}). \quad (1)$$

After applying the Galerkin method, a nonlinear system of equations (2) is deduced, which can be solved by an appropriate algorithm, such as the Newton method [7]

$$\mathbf{M}(\boldsymbol{X}(\theta))\boldsymbol{X}(\theta) = \boldsymbol{B}_{\text{Load}}(\theta). \quad (2)$$

III. Reduction Techniques

The resulting system of equations can be large and inherently leads to high computational efforts. While the POD copes with the solving of the system, the DEIM focuses on reducing the computational effort of building the nonlinear part of the system matrix.

A. Proper Orthogonal Decomposition

The fundamental idea of the POD is based on reconstructing a system by a set of linearly independent vectors, which spans an orthogonal basis in the solution subspace. For this purpose, a set of previously computed snapshots $\mathbf{A}_S = [X_1, X_2, \ldots, X_n]$ is decomposed by a singular value decomposition (SVD)

$$\mathbf{A}_S = \mathbf{U}\Sigma\mathbf{V}^T \quad (3)$$

to create a projection operator $\Psi \in \mathbf{R}^{\text{DOF}\times m}$, which is used to project the reference system of order DOF into the reduced system of order m. The snapshots can be computed in different ways such as equivalently distributed in the simulation interval or by greedy or constrained algorithms based on the quantity of interest [5]. The projection operator is defined by the m first columns of the left singular orthonormal matrix given by $\mathbf{U} \in \mathbf{R}^{\text{DOF}\times\text{DOF}}$ (3) [8], [10], [16]. The reduced system is consecutively achieved by

$$\Psi^T \boldsymbol{X}(\theta) = \boldsymbol{X}_r \quad (4)$$

$$\Psi^T \mathbf{J}(\boldsymbol{X}(\theta))\Psi\delta\boldsymbol{X}_r = \Psi^T \boldsymbol{R}(\boldsymbol{X}(\theta)) \quad (5)$$

Manuscript received November 29, 2020; revised February 3, 2021 and March 9, 2021; accepted March 24, 2021. Date of publication March 31, 2021; date of current version May 17, 2021. Corresponding author: F. Müller (e-mail: fabian.mueller@iem.rwth-aachen.de).

Color versions of one or more figures in this article are available at https://doi.org/10.1109/TMAG.2021.3070183.

Digital Object Identifier 10.1109/TMAG.2021.3070183

TABLE I
DEIM ALGORITHM

1. $[|p|, \phi_1] = max\{|\boldsymbol{w}_1|\}$
2. $\mathbf{W} = [\boldsymbol{w}_1],\ \mathbf{P} = [\boldsymbol{e}_{\phi_1}],\ \phi = [\phi_1]$
3. $\mathrm{k} = 1,\ R_\mathrm{k} = 1 - \frac{\sum_{\mathrm{i}=1}^{\mathrm{k}} \sigma_\mathrm{i}}{\sum_{\mathrm{i}=1}^{\mathrm{n}} \sigma_\mathrm{i}}$
4. While $R_\mathrm{k} > \alpha$ do:
5. $\quad \mathrm{k} = \mathrm{k} + 1,$
6. $\quad$ Solve $(\mathbf{P}^T \cdot \mathbf{W})\boldsymbol{c} = (\mathbf{P}^T \cdot \boldsymbol{w}_\mathrm{k})$ for $\boldsymbol{c}$
7. $\quad \boldsymbol{Residual} = \boldsymbol{w}_\mathrm{k} - \mathbf{W}\boldsymbol{c}$
8. $\quad [|p|, \phi_\mathrm{k}] = max\{|\boldsymbol{Residual}|\}$
9. $\quad \mathbf{W} \leftarrow [\mathbf{W}\ \boldsymbol{w}_\mathrm{k}],\ \mathbf{P} \leftarrow [\mathbf{P}\ \boldsymbol{e}_{\phi_\mathrm{k}}],\ \phi \leftarrow \begin{pmatrix} \phi \\ \phi_\mathrm{k} \end{pmatrix}$
10. $\quad R_\mathrm{k} = 1 - \frac{\sum_{\mathrm{i}=1}^{\mathrm{k}} \sigma_\mathrm{i}}{\sum_{\mathrm{i}=1}^{\mathrm{n}} \sigma_\mathrm{i}}$
11. end while

which is much smaller than the reference system. However, the evaluation of the residual $\boldsymbol{R}(\boldsymbol{X}(\theta))$ and the Jacobian matrix $\mathbf{J}(\boldsymbol{X}(\theta))$ still depend on the solution vector $\boldsymbol{X}(\theta)$ in the reference system.

B. Discrete Empirical Interpolation Method

When evaluating the residual and the Jacobian in the reference system, which is a significant computational burden, the DEIM can be utilized [8], [10]–[12]. This method evaluates the nonlinear terms on a small subset of elements connected to the interpolation indices. The DEIM algorithm can be improved by taking the information value of the snapshots into account given by the singular values σ to truncate the nonlinear basis. A measure of the relative energy E_k related to a singular value σ_k is given by

$$E_k = \frac{\sigma_k}{\sum_{i=1}^{n} \sigma_i}. \tag{6}$$

In order to construct a truncated optimal basis of order k, the residual relative energy R_k is expressed as

$$R_k = 1 - \frac{\sum_{i=1}^{k} \sigma_i}{\sum_{i=1}^{n} \sigma_i}. \tag{7}$$

This residual relative energy can consecutively be used as a threshold value for the DEIM process [8], [12]. The singular values are by definition decreasing, which enables to extract information about which singular vector will add new information to the decomposition [8]. The adapted DEIM algorithm is given in Table I. It should be remarked that the POD-DEIM will always be less accurate compared to a pure POD method. Only if the DEIM approximation is exact, the POD-DEIM is as accurate as the POD itself [14]. The resulting matrix $\mathbf{P}$ consists of the interpolation indices, while $\mathbf{W}$ is a basis of the nonlinear function subspace. The DEIM projection is consecutively applied to the residual and the Jacobian matrix [10]. The Gappy-POD reduces the instabilities of the DEIM by increasing the number of interpolation indices to be higher than the number of the nonlinear basis in $\mathbf{W}$ [10]. Another approach is proposed here by taking different projection bases to fully exploit magnetic field periodicities and local similar states of magnetic saturation in the machine [3], [6]. The approach assumes that a parameter, such as a rotor angle θ, strongly influences the nonlinear function. Nevertheless, solutions close to θ are similar to the one at θ. Arranging similar non-linear solutions in subsets and switching between the corresponding projections depending on θ further improves the reduced order model (ROM). Employing a small local basis for rotor angle intervals with a width of half a pole leads to smaller projection operators; however, multiple SVDs are needed to create the different projections leading to a slightly higher computational effort compared to taking one large projection basis. Due to the fact that no algorithm for the determination of the local subsets is used, our approach is only a rudimentary implementation of the LDEIM [3].

TABLE II
MACHINE DATA

Data	
Rated power	30 kW
Rated torque	100 Nm
Rated speed	3000 rpm
Number of pole pairs	3
Phases	3
Length	80 mm
Magnet remanence	1.2 T

IV. APPLICATION ON SYNCHRONOUS MACHINE

In Section IV, the proposed reduction techniques are applied to a synchronous machine with buried permanent magnets, which is used as a traction drive for electric vehicles. The machine data are given in Table II. The simulation is conducted over 0°–120° in 180 angular steps, and the snapshots are taken for an operating point at $(I_d, I_q) = (-4.6, 4.7)$ A/mm^2 at a distinct number of n equivalently distributed rotor angles. In the following analysis, the representation of typical machine characteristics, such as torque and iron losses, is presented. First, the Gappy POD, DEIM with the proposed truncation criteria based on α, and LDEIM are applied to the machine simulation with 60 and 90 snapshots. It has to be remarked here that the simulation of the Gappy and DEIM did not converge without truncation. In our simulations, the threshold value for the truncation α is set to $0.1 \cdot 10^{-3}$. The accuracy of the different ROMs is evaluated by assessing the absolute residual of the simulation in each angular step and averaging them. Table III holds the results for the different methods. It can be depicted that the Gappy POD is as accurate as of the DEIM and more stable, which underlines the findings in [10]. The LDEIM, which employs a smaller local basis, shows the best accuracy compared to the Gappy POD and truncated DEIM. The following evaluation of machine parameters is due to the empirical evaluation of a reasonable truncation factor for the DEIM and Gappy POD and the better accuracy of the LDEIM only conducted for the POD and POD-LDEIM. If higher accuracy is necessary, a method given by [15] might be interesting, which reformulates the magnetic vector potential formulation into a quadratic bilinear algebraic form. However, most electromagnetic finite-element software packages are not capable of using higher order tensors.

A. Local Flux Density Distribution

The first analysis is performed with a focus on the local flux density distribution. This is particularly important because it is

TABLE III
AVERAGE ABSOLUTE ERROR IN PERCENT

	ϵ_{ave}		No. DEIM Nodes	
No. Snapshots	60	90	60	90
Method				
POD	8.06	1.84	0	0
DEIM	11.05	diverged	43	76
Gappy	11.06	4.99	46	76
LDEIM	9.63	2.56	60	85

the starting point for the post-processing of the iron losses and torque. The deviation between the reference solution and POD reaches higher values at angular steps, which are not included in the snapshots. Furthermore, the DEIM approximates the representation of the nonlinear material by an interpolation, which increases the error. The local deviation between the full and reduced models' solution is shown in Fig. 1 for an angular step of $\theta = 0.66°$, which is not used as a snapshot. The vector potential and the flux density are illustrated. It is noticeable that the difference between the reference vector potential and POD vector potential $\boldsymbol{A}_{\text{Ref}} - \boldsymbol{A}_{\text{POD}}$ [see Fig. 1(c)] is smaller than the deviation given by $\boldsymbol{A}_{\text{Ref}} - \boldsymbol{A}_{\text{POD-LDEIM}}$ [see Fig. 1(d)]. The flux density is a post-processed quantity and, therefore, shows the same behavior. Although local deviations occur, the overall field distribution is a good approximation of the reference field. The major part of the deviations of the POD, as shown in Fig. 1(e), occurs on the surface of the machine's rotor, the airgap, and the teeth tips. Minor deviations occur in the stator. The POD-LDEIM depicted in Fig. 1(f) shows larger overall deviations with a similar local distribution in the rotor. It is noticeable that the interpolation introduces locally higher errors, which underlines the tradeoff between computation savings in terms of DOF and achievable accuracy.

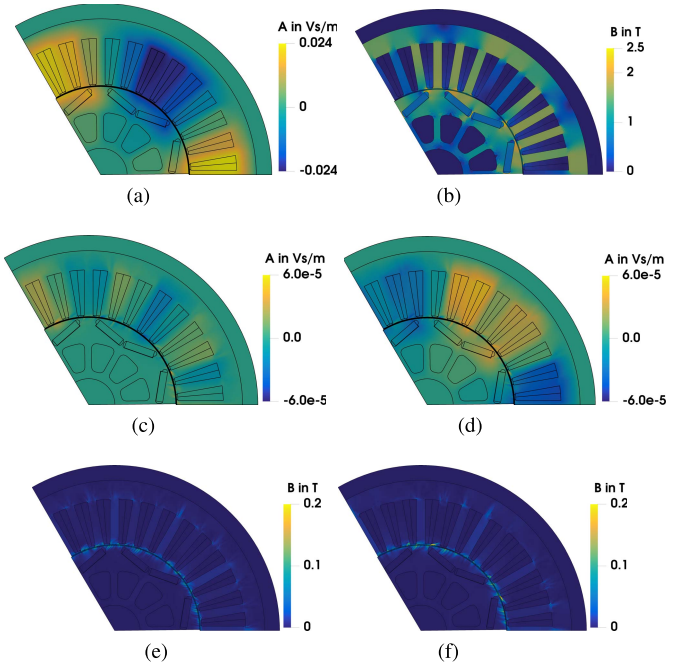

Fig. 1. Comparison of ROMs' vector potential and flux density approximations and reference vector potential and flux density. (a) Reference vectorpotential $\boldsymbol{A}_{\text{Ref}}$. (b) Reference flux density $\boldsymbol{B}_{\text{Ref}}$. (c) $\boldsymbol{A}_{\text{Ref}} - \boldsymbol{A}_{\text{POD}}$. (d) $\boldsymbol{A}_{\text{Ref}} - \boldsymbol{A}_{\text{POD-LDEIM}}$. (e) $\boldsymbol{B}_{\text{Ref}} - \boldsymbol{B}_{\text{POD}}$. (f) $\boldsymbol{B}_{\text{Ref}} - \boldsymbol{B}_{\text{POD-LDEIM}}$.

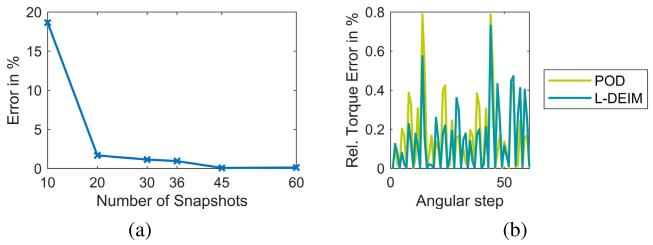

Fig. 2. Torque errors for ROMs using 60 snapshots. (a) Error of average torque versus number of snapshots for POD. (b) Relative torque error in %.

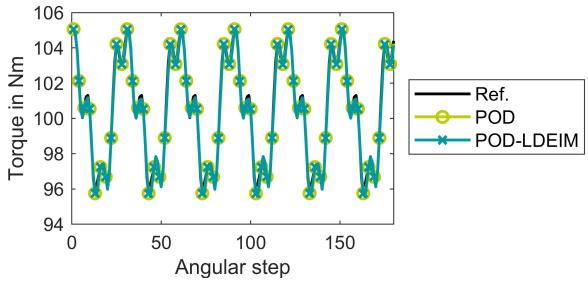

Fig. 3. Torque versus angular steps for different simulation techniques with 60 snapshots. Markers indicate steps that are included in the snapshot set.

B. Torque

The second comparison is conducted for the torque as a globally integrated quantity. In Fig. 2(a), the average torque error for different numbers of snapshots is shown, and it can be seen that at least 45 snapshots are necessary for the POD to accurately reproduce the torque with an error of less than 0.1%. To have a reasonable mathematical accuracy of the reduced model, 60 steps are taken (see Table III). In Fig. 2(b), the relative error is depicted for each angular position for the first 60 steps. The error is for all steps smaller than 1%, but the better mathematical accuracy of the POD cannot be recognized in the relative torque deviation. A direct comparison of the torque versus the angular step of the three computation methods in Figs. 2(a) and 3 shows that the POD produces as precise results as the POD-LDEIM even though the mathematical residual is smaller (see Table III), but it is not beneficial in terms of computational effort, as stated in Section III.

C. Iron Losses

The iron losses of the machine are computed by the IEM 5-parameter iron loss formula [1], [13]

$$P_{\text{IEM}} = a_1 B^{\alpha} f + a_2 B^2 f^2 (1 + a_3 B^{a_4}) + a_5 B^{1.5} f^{1.5} \quad (8)$$

with f being the frequency and a_1–a_5 material-dependent loss parameters. For this purpose, the magnetic flux density frequencies are determined by a Fourier decomposition to use the frequency dependent formula. As shown in Section IV-B, local errors occur introducing numerical noises and additional frequencies in the decomposition. Even though the numerical noise results in an error of the flux density frequencies,

TABLE IV
IRON LOSSES

Method	Rotor losses in W	Stator losses in W
Reference	13.8	198.1
POD	13.7	198.3
POD-LDEIM	13.6	199.6

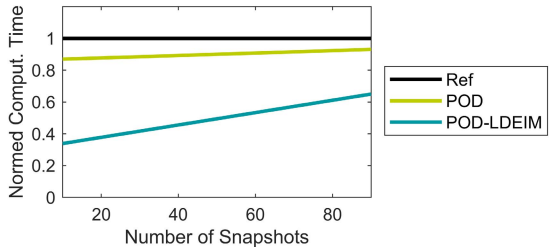

Fig. 4. Normed computational effort for the simulated VPMSM.

the approximated iron losses are in good agreement with the reference losses. The reason for this is given by the terms on which the numerical noises act and the location of the losses. The main terms, which are affected by the numerical noise, are of order larger ones, namely, the eddy current and excess losses. By using thin electrical steel sheets, the coefficients belonging to these terms are rather small, resulting in a minor influence on the computed losses depicted in Table IV. Furthermore, the main part of the deviations is located near the airgap. The rotor iron losses of a synchronous machine are small compared to the stator losses. In major parts of the stator, only small deviations occur, which leads to only a minor influence on the stator losses. As the local flux density deviation from Fig. 1(e) indicates, the POD is nearly similar to the reference, but, even though the POD-LDEIM shows stronger deviations [see Fig. 1(f)], the iron losses are still accurate enough. In Fig. 4, the computational time for the different methods is given. All simulations have been conducted on a single core, and the reference time is normalized. In the case of the problem analyzed in this contribution, the additional multiplications in the POD lessen the computational saving to 10%. The POD-LDEIM shows a lower computational effort because of the additional reduction of the nonlinear terms. The calculation of a solution for a distinct time step after the snapshots has been computed and the projections are created is three times faster than the reference. Taking the snapshot calculation into account, a computational saving of 45% is obtained if 60 snapshots are used.

V. CONCLUSION

In this contribution, a comparison between different DEIM methods and Gappy POD applied to a synchronous machine is given. Employing local projections as in the LDEIM offered the highest accuracy and is stable. It is shown that the ROM is able to approximate the machine behavior in terms of torque and losses as globally integrated quantities. Local quantities can show deviations due to the interpolation approach. Particularly, in the first geometry design steps of electrical machines, where the required accuracy is not as high as in the final design process, ROMs offer an efficient way to approximate the machine behavior.

ACKNOWLEDGMENT

This work was supported by the German Research Foundation (DFG) under research project 347941356 "Numerical Analysis of Electromagnetic Fields by Proper Generalized Decomposition in Electrical Machines."

REFERENCES

[1] S. Steentjes, G. von Pfingsten, M. Hombitzer, and K. Hameyer, "Iron-loss model with consideration of minor loops applied to FE-simulations of electrical machines," *IEEE Trans. Magn.*, vol. 49, no. 7, pp. 3945–3948, Jul. 2013.

[2] B. Peherstorfer, Z. Drmač, and S. Gugercin, "Stability of discrete empirical interpolation and Gappy proper orthogonal decomposition with randomized and deterministic sampling points," *SIAM J. Sci. Comput.*, vol. 42, no. 5, pp. A2837–A2864, Sep. 2020.

[3] B. Peherstorfer, D. Butnaru, K. Willcox, and H.-J. Bungartz, "Localized discrete empirical interpolation method," *SIAM J. Sci. Comput.*, vol. 36, no. 1, pp. A168–A192, Jan. 2014.

[4] E. Lange, F. Henrotte, and K. Hameyer, "A variational formulation for nonconforming sliding interfaces in finite element analysis of electric machines," *IEEE Trans. Magn.*, vol. 46, no. 8, pp. 2755–2758, Aug. 2010.

[5] V. Mukherjee, M. F. Far, F. Martin, and A. Belahcen, "Constrained algorithm for the selection of uneven snapshots in model order reduction of a bearingless motor," *IEEE Trans. Magn.*, vol. 53, no. 6, pp. 1–4, Jun. 2017.

[6] Y. Sato, M. Clemens, and H. Igarashi, "Adaptive subdomain model order reduction with discrete empirical interpolation method for nonlinear magneto-quasi-static problems," *IEEE Trans. Magn.*, vol. 52, no. 3, pp. 1–4, Mar. 2016.

[7] J. Saitz, "Newton–Raphson method and fixed-point technique in finite element computation of magnetic field problems in media with hysteresis," *IEEE Trans. Magn.*, vol. 35, no. 3, pp. 1398–1401, May 1999.

[8] L. Montier, T. Henneron, S. Clénet, and B. Goursaud, "Transient simulation of an electrical rotating machine achieved through model order reduction," *Adv. Model. Simul. Eng. Sci.*, vol. 3, no. 1, pp. 1–17, Dec. 2016.

[9] A. Hochman, B. N. Bond, and J. K. White, "A stabilized discrete empirical interpolation method for model reduction of electrical, thermal, and microelectromechanical systems," in *Proc. 48th ACM/EDAC/IEEE Design Automat. Conf. (DAC)*, New York, NY, USA, Jun. 2011, pp. 540–545.

[10] M. R. Hasan, L. Montier, T. Henneron, and R. V. Sabariego, "Stabilized reduced-order model of a non-linear eddy current problem by a Gappy-POD approach," *IEEE Trans. Magn.*, vol. 54, no. 12, pp. 1–8, Dec. 2018.

[11] F. Ghavamian, P. Tiso, and A. Simone, "POD–DEIM model order reduction for strain-softening viscoplasticity," *Comp. Methods Appl. Mech. Eng.*, vol. 317, pp. 456–479, Apr. 2017.

[12] S. Chaturantabut and D. C. Sorensen, "Nonlinear model reduction via discrete empirical interpolation," *SIAM J. Sci. Comput.*, vol. 32, no. 5, pp. 2737–2764, Jan. 2010.

[13] N. Leuning, S. Elfgen, B. Groschup, G. Bavendiek, S. Steentjes, and K. Hameyer, "Advanced soft- and hard-magnetic material models for the numerical simulation of electrical machines," *IEEE Trans. Magn.*, vol. 54, no. 11, pp. 1–8, Nov. 2018.

[14] D. Wirtz, D. C. Sorensen, and B. Haasdonk, "A posteriori error estimation for DEIM reduced nonlinear dynamical systems," *SIAM J. Sci. Comput.*, vol. 36, no. 2, pp. A311–A338, Jan. 2014.

[15] D. Klis, S. Burgard, O. Farle, and R. Dyczij-Edlinger, "A self-adaptive model-order reduction algorithm for nonlinear eddy-current problems based on quadratic-bilinear modeling," *IEEE Trans. Magn.*, vol. 52, no. 3, pp. 1–4, Mar. 2016.

[16] D. Schmidthausler and M. Clemens, "Low-order electroquasistatic field simulations based on proper orthogonal decomposition," *IEEE Trans. Magn.*, vol. 48, no. 2, pp. 567–570, Feb. 2012.